The 2019 World Congress on
Advances in Structural Engineering and Mechanics (ASEM19)
Jeju Island, Korea, September 17 - 21, 2019

Effect of screw spacing on axial strength of cold-formed steel built-up box sections-numerical investigation and parametric study

*Krishanu Roy[1)], Hieng Ho Lau [2)], Boshan Chen[3)],Tina Chui Huon Ting [4)], and James B.P. Lim [5)]

[1), 3), 5)] *Department of Civil and Environmental Engineering, The University of Auckland, New Zealand*
[2)] *Faculty of Engineering, Computing and Science Swinburne University of Technology, Sarawak Campus, Kuching, Sarawak, Malaysia*
[4)] *Faculty of Engineering and Science, Curtin University Malaysia, Miri, Sarawak, Malaysia*
[1)] kroy405@aucklanduni.ac.nz

ABSTRACT

In cold-formed steel (CFS) structures, the use of built-up box sections are becoming increasingly popular for column members. Applications of CFS built-up box sections include in steel trusses, space frames, and portal frames. This paper considers the finite element modelling of built-up CFS box sections under axial compression. The FE models considered nonlinear material properties, initial imperfections and modeling of intermediate fasteners. The FE results showed good agreement against the laboratory test results reported in other study for such CFS built-up box sections. The validated FE model was then used to conduct a parametric study comprising 148 models. The effect of screw spacing on the axial capacity, was investigated. Both the finite element and laboratory test results were compared against the design strengths calculated in accordance with the American Iron and Steel Institute (AISI) and Australian and New Zealand Standards (AS/NZS). From the comparison, it was observed that the AISI & AS/NZS are conservative by around 17% while determining the axial capacity of such built-up CFS box columns.

1. INTRODUCTION

Structural applications of cold-formed steel (CFS) sections are very common in low and medium rise buildings nowadays and the use of CFS built-up box sections is becoming popular. This paper presents the results of 148 finite element analyses on CFS built-up box sections; The cross-sectional details of the CFS built-up box section are shown in Figure 1. As can be seen, the CFS built-up box section is formed using two identical lipped channel-sections connected front-to-front. Such CFS built-up box sections are used in CFS construction due to the advantages of high load-carrying capacity, stability, and higher moment of inertia, as compared to the back-to-back built-up CFS channel sections.

[1)] PhD Scholar
[2)] Professor
[3)] PhD Scholar
[4)] Lecturer
[5)] Professor

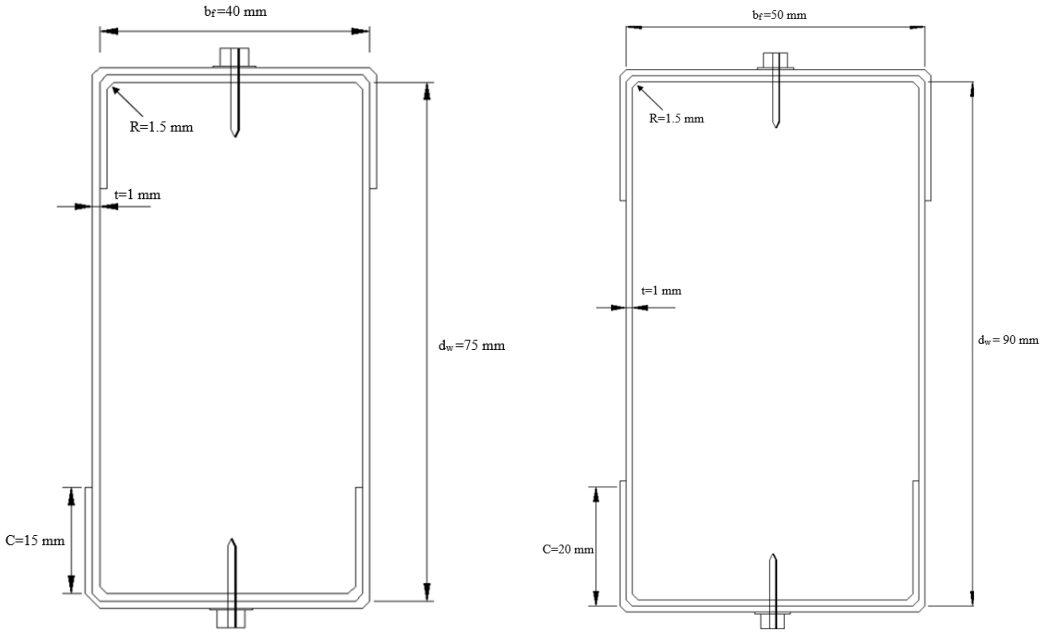

(a) B75 (b) B90

Fig. 1: Nominal cross-sections of CFS built-up box sections considered in this paper

In the literature, limited research work has described for CFS built-up box sections, composed of channels, connected front-to-front through bolts or screws, under axial compression. However, numerous works can be found in the literature for CFS built-up channels connected back-to-back under compression, including recent work of the authors (Roy *et al*. 2018a, b, c, d, 2019a, b, c, d). Ting *et al*. (2018) studied the behavior of CFS built-up channels, connected back-to-back under axial compression (Figure 2 (a)). To extend this work, Roy *et al*. (2018 b), experimentally investigated the axial capacity of CFS built-up channels, connected back-to-back with a gap (Figure 2 (b)). Crisan *et al*. (2014) previously presented numerical models on built-up sections connected back-to-back with battens/stitches. Rondal and Niazi (1990) conducted full-scale experiments to determine the axial capacity of CFS built-up columns, connected back-to-back with spacers and stitches. Recently, Roy *et al*. (2018d) presented a FE investigation on the axial capacity of CFS built-up un-lipped channels screwed back-to-back, concluding that AISI & AS/NZS can be un-conservative for stub columns (Figure 2(c)). It should be noted that most of the researchers as discussed above, focussed on the behaviour of back-to-back built-up channels because of the ease in connection between the back-to-back channels. Whereas, this paper presents a numerical investigation on axial capacity of CFS built-up box sections. The FE models considered nonlinear material properties and initial imperfections. A total of 148 finite element

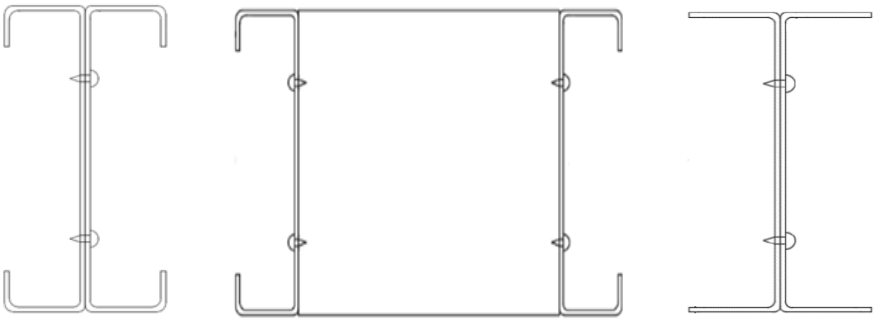

(a) Ting et al. (2018) (b) Roy et al. (2018 b) (c) Roy et al. (2018 d)

Fig. 2: Built-up cold-formed steel columns from literature

models were developed to investigate the effect of fastener spacing on axial strength of such CFS built-up box columns. Two different cross sections of the built-up box columns (B75 and B90) were considered in the parametric study (Figure 1). The axial capacity and deformation patterns of CFS built-up columns are reported. The finite element results were compared against the design strengths calculated in accordance with the American Iron and Steel Institute (AISI) and Australian and New Zealand Standards (AS/NZS).

2. SUMMARY OF EXPERIMENTAL WORK

The finite element models, developed in this study, were validated against the test results by Roy *et al*. (2019 a). Roy *et al*. (2019 a) presented compression tests on both the single channel and CFS built-up box sections. More experimental details can be found in Roy *et al*. (2019 a). A brief summary of the tests reported by Roy *et al*. (2019 a) is described in this section.

The cross-sectional details of the CFS single channel and built-up box sections considered in this paper: C75, and B75, are shown in Figure 1. B75 is the built-up section from C75 channels. In this study, intermediate fasteners were used to connect the flanges of the front-to-front channels to form the built-up box section. The dimensions of the built-up box sections and single channel sections are summarized in Table 1. The built-up columns were subdivided into two different column heights: short columns of 0.5 m height and slender columns of 1.5 m height. Pin-ended boundary conditions were applied for all single channel and built-up columns tested herein. In the test programme, longitudinal screw spacing of 100 mm was considered for all columns.

Table 1 Cross sectional dimensions and experimental and FEA results

(a) C75 (Single lipped channel section)

Specimen	Web d_w (mm)	Flange b_f (mm)	Lip C (mm)	Length L (mm)	Test result P_{EXP} (mm)	FEA result P_{FEA} (mm)	P_{FEA} /
Short							

C75- L500-1	75.0	38.1	14.0	500.2	57.5	59.8	1.04
C75- L500-2	76.1	40.0	14.1	501.1	55.5	56.6	1.02
C75- L500-3	75.4	39.4	15.2	503.2	54.2	55.8	1.03
C75- L500-4	74.8	39.4	15.6	499.7	57.7	60.0	1.04
Slender							
C75- L1500-1	76.3	41.2	15.4	1500.1	39.0	39.8	1.02
C75- L1500-2	74.7	40.6	14.7	1502.4	40.5	41.7	1.03
C75- L1500-3	75.4	39.7	16.1	1498.4	42.0	43.3	1.03
C75- L1500-4	74.8	39.2	15.8	1507.2	45.5	47.8	1.05

(b) B 75 (Built-up box section)

Specimen	Web d_w (mm)	Flange b_f (mm)	Lip C (mm)	Length L (mm)	Test result P_{EXP} (mm)	FEA result P_{FEA} (mm)	P_{FEA} / P_{EXP}
Short							
B75- L500-1	76.1	39.8	15.1	500.4	124.8	128.6	1.03
B75- L500-2	75.2	38.5	14.2	498.7	127.5	132.5	1.04
B75- L500-3	74.7	41.6	14.8	499.6	130.5	133.3	1.02
B75- L500-4	77.2	40.2	14.2	502.4	129.7	137.2	1.06
Slender							
B75- L1500-1	77.4	41.2	14.4	1500.9	88.4	92.7	1.05
B75- L1500-2	76.4	40.6	14.6	1502.6	89.7	95.7	1.07
B75- L1500-3	75.4	39.7	15.3	1507.4	91.4	95.9	1.05
B75- L1500-4	75.2	38.7	15.1	1511.4	92.7	99.8	1.08

Type of the built-up section, nominal specimen length, and test specimen number was coded by the specimen labelling. For example, the label “B75-L1500-1”, as shown in Figure 3, indicates the depth of the channel section is 75 mm. B stands for the built-up box section and L indicates the specimen length as is 1500 mm. At the end of the label, the number 1 is used to express the specimen number as 1.

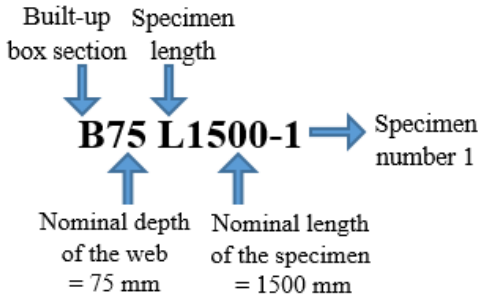

Fig. 3: Specimen labelling

In order to determine the material properties of the steel, tensile coupons were cut from both the longitudinal and transverse directions. All the coupons were then tested according to British standard BS EN (2001). Average initial and full stress-strain curves of the steel determined from the coupon tests are shown in Figure 4(a) and Figure 4(b), respectively. From the results of tensile coupon tests for longitudinal

and transverse coupons, average values of the E and F_y were 207 N/mm^2 and 559 N/mm^2, respectively (Table 2).

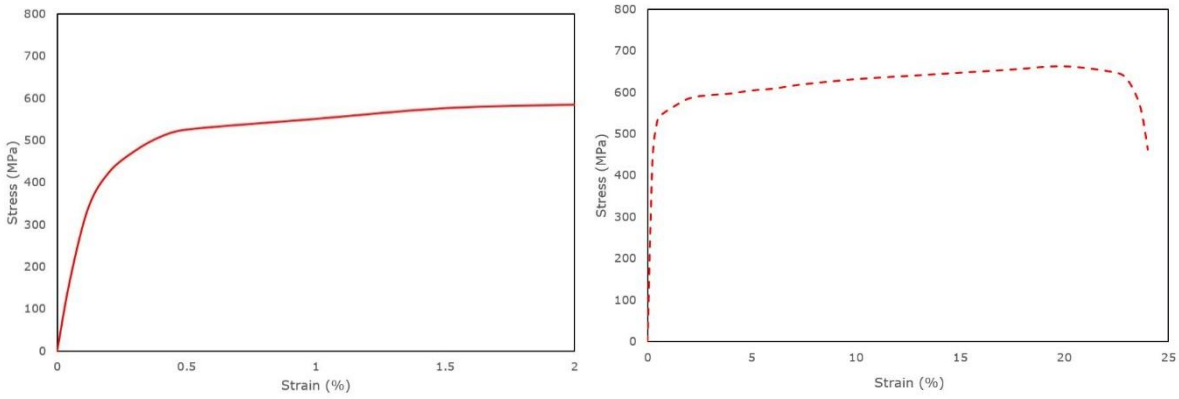

(a) Initial stress–strain curve (b) Full stress–strain curve

Fig. 4: Initial and final stress-strain curves of the CFS used in this research

Table 2 Material properties obtained from tensile coupon tests

Section	Nominal thickness	Base metal thickness	Gauge length	Yield stress	Gauge width	Ultimate stress	Young's modulus
	t	T	L_0	$\sigma_{0.2}$	b	σ_u	E
	(mm)	(mm)	(mm)	(MPa)	(mm)	(MPa)	GPa
Longitudinal	1.01	1.0	50	559	12.5	678	207

All the built-up box sections and single channels were loaded using a Universal Testing Machine (UTM) (Figure 5). Pin-ended boundary conditions were applied for all single channel and built-up columns tested herein. In order to ensure there was no gap between the two pin-ends and end plates of the specimen, all columns were loaded initially up to 25% of their expected failure load and then released. All columns were loaded under displacement control, with a displacement rate of 0.03 mm/s (Figure 6). Load was applied through the centre of gravity (CG) of the specimens. Four LVDTs were used for all built-up column tests. LVDT positions are shown in Figure 7. One LVDT was used in the longitudinal direction to measure the axial shortening, while all other LVDTs were used in the transverse direction, to measure the lateral displacement of the built-up columns. With each increment of loading, LVDT readings were recorded, until the ultimate failure of single-channel and built-up box sections

occurred. A load cell was installed at the top of the base plate, which was used to record the failure load. The axial load and the readings of the transducers were recorded by a data acquisition system at regular intervals during the tests.

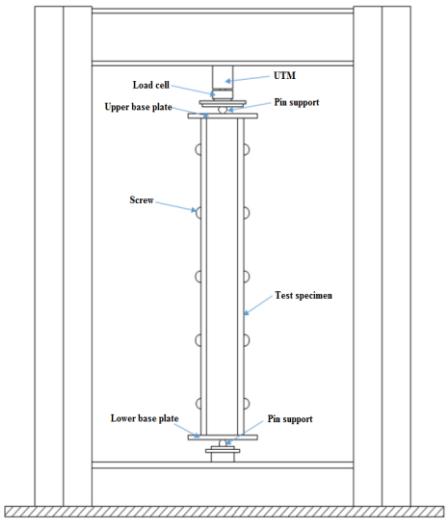

Fig. 5: Drawing of loading test-rig

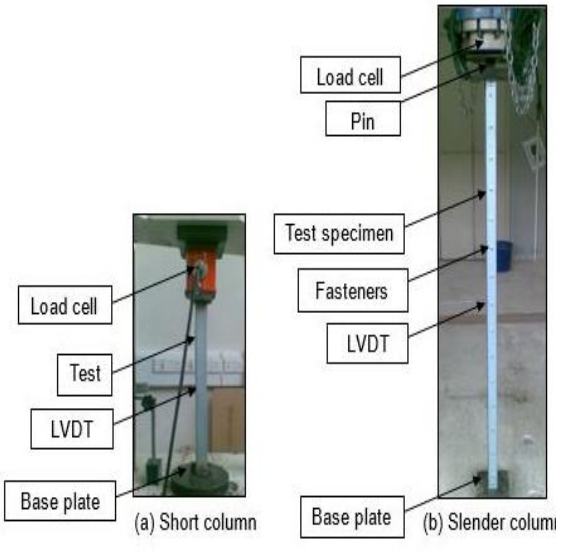

Fig. 6: Test set-up for short and slender columns

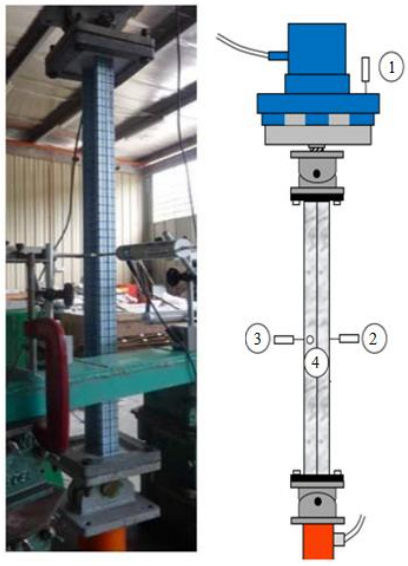

Fig. 7: Position of LVDTs (slender column tests

Prior to compression testing, a total station assembly was used to measure the initial imperfections present in the built-up columns (Figure 8(a)). In Figure 8(b), initial imperfections are plotted against the length of the B75-L500-1. The maximum imperfections of single channels and built-up box sections are shown in Table 3. These values of overall imperfections given in Table 3, were measured in the middle of the flanges, webs and lips of each channel and built-up sections and the average of the maximum values were considered.

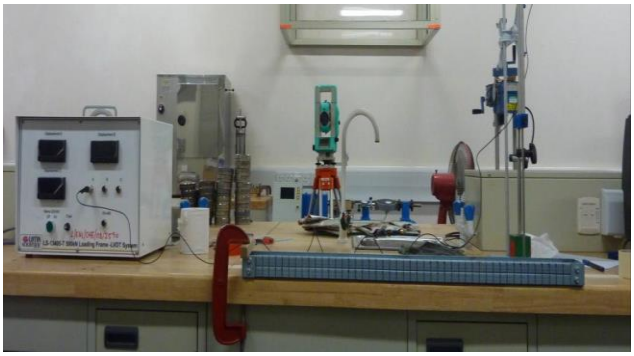

(a) Imperfection measurement setup

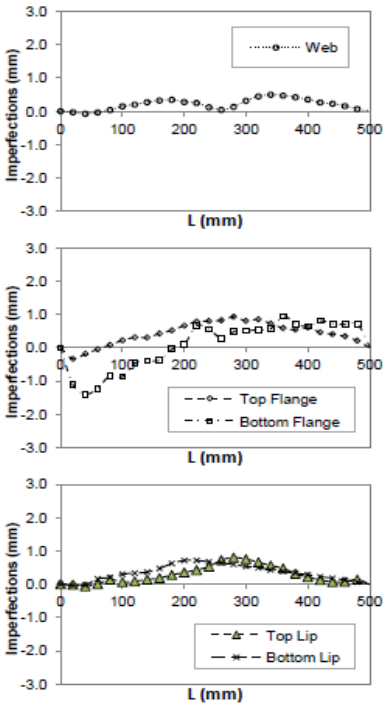

(b) Typical imperfection profile for B75-L500-1

Fig. 8: Details of imperfection measurements from experimental investigation

3. NUMERICAL INVESTIGATION

3.1 General

ABAQUS (2018) was used to develop nonlinear elasto-plastic FE models for both, CFS single channel and built-up box sections. The modeling techniques were described by Lian et al. (2016a, b) for back-to-back sections. Centre line dimensions of the cross-sectional geometry were used in the FE model. Full geometries were modeled for all test specimens. Screws were also modeled between the flanges of two-channel sections, forming the built-up box section. In the FE model, only the fastener head was modeled, which was connected to the flanges of front-to-front channels. Specific modeling techniques are discussed in detail as below.

3.2 Analysis procedure

Two different methods of analysis were used to model single channel and CFS built-up box sections: elastic buckling and nonlinear static RIKS method. Elastic buckling analyses were used to obtain the eigenvectors for modeling the initial imperfections. Nonlinear static RIKS analysis was used to apply the axial load on the single channel and CFS built-up box sections. The RIKS method is generally used to predict unstable, geometrically nonlinear collapse of a structure. It often follows an eigenvalue buckling analysis to provide complete information about a structure's collapse and can be used for post-buckling analysis and speed convergence of ill-conditioned or snap-through buckling problems that do not exhibit instability. Therefore, general RIKS was preferred over the general static as the analysis method (ABAQUS, 2018).

3.3 Material modelling

An elastic-plastic model was used for modeling the overall geometry of the built-up sections and single channels. In order to define the isotropic yielding and plastic hardening of the steel, the von Mises yield surface was used in the classical metal plasticity model. These material models were used by the authors in their previous research on CFS built-up columns, which gave good correlation against the experimental test results in Roy *et al*. (2019a). However, it is to be mentioned that the orthotropic material behaviour was not considered in the FE model to avoid the complexity of the analysis. The material properties were taken from the tensile coupon tests and included in the FE models. Tensile coupon tests show, the average values of yield strength, ultimate stress and Young's modulus of elasticity were 559 MPa, 678 MPa, and 207 GPa, respectively.

3.4 FE meshing and element type

S4R shell elements were used to model the single channel and built-up columns. S4R elements allow each node to have three degrees freedom both along translational and rotational directions. S4R elements are suitable for the analysis of nonlinear problems as it accounts for finite membrane strains and arbitrarily large rotation. Rigid quadrilateral shell elements (R3D4) were used to model the upper and lower endplates. In order to model the screw head, three-dimensional eight-noded continuum elements were used with a mesh size of 2 mm by 2 mm. Across the length and width, a mesh size of 5 mm × 5 mm was used for the convergence of both single channel sections and built-up box sections. Also, for the top and bottom base plate, a mesh size of 5 mm × 5 mm was used. Typical FE meshing is shown in Figure 9 (ii) for B75-a100-L500-1, where “a100” is the spacing between the fasteners as 100 mm.

3.5 Modeling of boundaries and loading procedure

Pin-pinned boundaries were applied in all FE models for both the single channel and CFS built-up box sections considered in this study. Two rigid plates were used at top and bottom ends of the built-up and single channel sections to simulate the laboratory test setup. Pin-pin boundary condition was modeled by applying rotations and displacements to both the end plates through a reference point. The reference point was considered as the CG of the cross-section of built-up box sections and single

channels. Applied boundary conditions in the FE model are shown in Figure 9 (i) for B75-a100-L500-1. All three translations were constrained against at the top layer nodes of the screw heads. Constraint conditions between the flanges of front-to-front channels and the fastener head were modeled adequately, so there is no slip between the front-to-front channels and the fasteners heads and the fasteners act as a rigid body. Master-slave contact pair option, available in ABAQUS library (2018), was used between the front-to-front channels. Also, between the fastener head and top channel, master-slave contact pair was modeled. The stiffness of the fasteners between the front-to-front channels was modeled using MPC beam connector elements available in the ABAQUS library. Displacement control static RIKS method (2018), was used to apply the axial load through the reference point of the top base plate (Figure 9 (i))

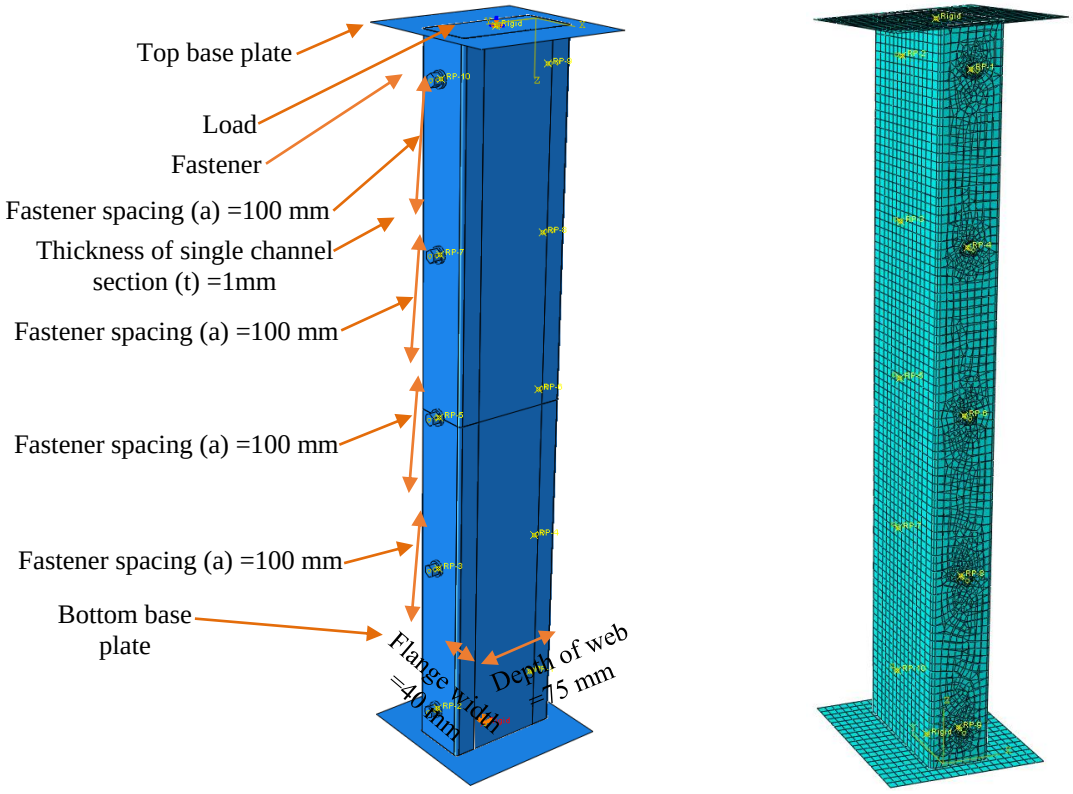

(i) Boundary condition applied in FE model (ii) Finite element mesh

Fig. 9: Details of typical finite element model (B75-a100-L500-1

3.6 Contact modeling

"Surface to surface" contact was used for modeling the interaction between the flanges of front-to-front channels. The web of one channel section was modeled as slave surface, while the web of other channel was considered as the master surface. There was no penetration between the two contact surfaces.

3.7 Initial imperfection modeling

Buckling behavior of single channel and CFS built-up box sections are dependent on many factors which include the ratio of length to thickness (L/t), flange width-thickness ratio (B/t) and lip-thickness ratio (C/t). Initial imperfections were considered in the FE modeling. Superimposition of local and overall imperfections was considered for accurate FE analysis. For all built-up box sections and single channel columns, Eigenvalue analyses were performed. For local buckling very small channel thickness was considered, however, for overall buckling, large channel thickness was used in the FE models. For local and overall buckling modes, lowest Eigenmode was used in ABAQUS (2018). The overall imperfections used in the modeling of built-up box sections and single channels were adjusted to the values measured from the experiments (Table 3). These values of overall imperfections given in Table 3, were measured in the middle of the flanges, webs and lips of each channel and built-up sections and the average of the maximum values were considered (Table 3). In addition, local imperfections of magnitude 0.5% of the section thickness were incorporated as recommended by Ellobody and Young (2005). In Figures 10, initial buckling modes are shown for B75-a100-L500-1. Similar modeling technique is described in the literature for CFS built-up columns by past researchers like Ellobody and Young (2007), to model local and overall imperfections.

Table 3 Maximum initial overall imperfections present in single channels and CFS built-up box sections

(a) C75

Specimen	Maximum initial imperfections (mm)
Short	
C75- L500-1	0.36
C75- L500-2	0.58
C75- L500-3	0.45
C75- L500-4	0.47
Slender	
C75- L1500-1	0.66
C75- L1500-2	0.62
C75- L1500-3	0.51
C75- L1500-4	0.59

(b) B75

Specimen	Maximum initial imperfections (mm)
Short	
B75- L500-1	0.16
B75- L500-2	0.18
B75- L500-3	0.15
B75- L500-4	0.17
Slender	

B75- L1500-1	0.23
B75- L1500-2	0.21
B75- L1500-3	0.20
B75- L1500-4	0.18

(a) Local buckling (b) Overall buckling

Figure 10: Initial imperfection contours (Eigen mode 1) for B75-a100-L500-1

3.8 Validation of the FE model

In Table 1, the failure loads for C75 and B75 columns from experiments and FE analysis are compared. The comparison shows that the FE results were close to the experimental results (Roy *et al*. (2019 a), both in terms of ultimate loads and observed buckling modes. Figures 11(a) and 11(b) shows the deflected shapes of the short and slender columns of single channel section (C75), obtained from the FE analysis. As can be seen, FE model's deflected shapes are similar to the experimental results. On the other hand, Figures 12(a) and 12(b) compares the failure modes of built-up box sections, obtained from the FEA and experiments. Load-axial shortening behavior, from both FEA and experiments, is plotted in Figures 13(a) and 11(b) for a single channel (C75) and built-up box section (B75), respectively. As can be seen from the graphs, FEA results are in good agreement with the experimental strengths. In addition, load versus lateral displacement curve is plotted in Figure 14 for B75, which showed a good comparison between FEA and experimental results, at mid-length of the built-up column.

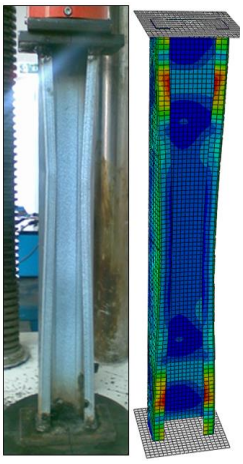

(i) Experimental (ii) FEA

(a) C75-L500-1

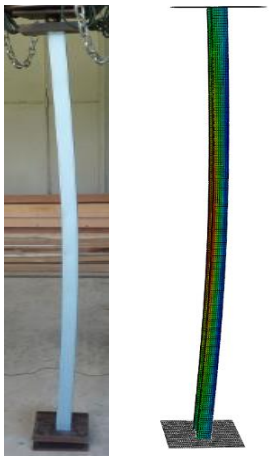

(i) Experimental (ii) FEA

(b) C75-L1500-1

Fig. 11: Deformed shapes of CFS single channel sections at failure

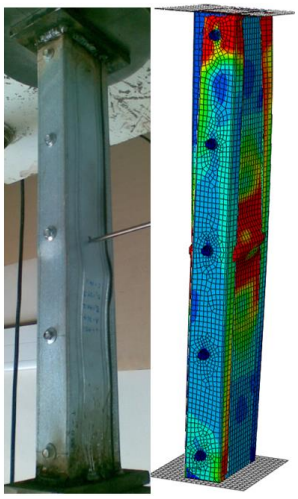

(i) Experimental (ii) FEA

(a) B75-L500-1

(i) Experimental (ii) FEA

(b) B75-L1500-1

Fig. 12: Deformed shapes of CFS built-up box sections at failure

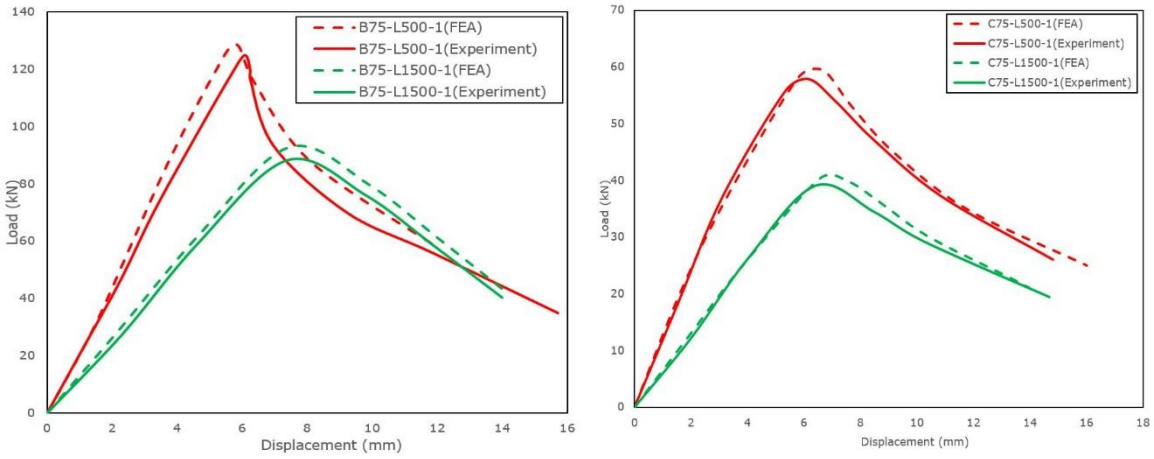

(a) C75 (b) B75

Fig. 13: Load versus axial displacement curves for CFS single channel and built-up box sections

Similar modelling techniques were considered for the back-to-back gapped built-up CFS channel sections under axial compression (Roy *et al*. 2018b), where the behaviour of the developed FE model agreed well with the experimental results. As the modelling techniques used in the previously developed FE model for back-to-back gapped built-up CFS channel sections, are similar to the modelling techniques described in this paper for CFS built-up box sections, the validated FE model described herein can be used for further study.

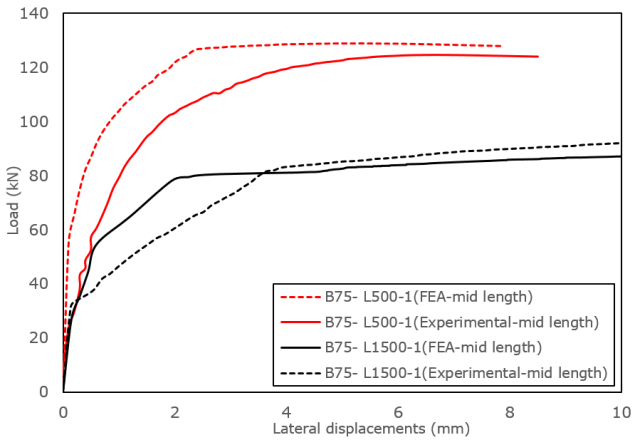

Fig. 14: Load versus lateral displacements relationship for CFS built-up box sections

4. PARAMETRIC STUDY

A parametric study, comprising 148 FE models was carried out to understand the effect of fastener spacing on the axial capacity of CFS built-up box sections. A wide range of slenderness, covering stub to slender columns was considered. Two different cross-sections i.e. B75 and B90 (Figure 1) were considered in the parametric study. Column lengths from 300 mm (stub) to 2000 mm (slender) were considered. Built-up

columns considered in the parametric study include four different columns heights: 0.3 m, 0.5 m, 1.0 m and 2.0 m as shown in Tables 4(a) and 4(b) for B75 and B90 columns, respectively. The fastener spacing's (a), considered in the parametric study, are as follows:

- Columns of 0.3 m height; screw spacing of 0.05 m, 0.1 m and 0.2 m
- Columns of 0.5 m height; screw spacing of 0.1 m, 0.2 m, and 0.4 m
- Columns of 1.0 m height; screw spacing of 0.225 m, 0.450 m, and 0.9 m
- Columns of 2.0 m height; screw spacing of 0.475 m, 0.950 m, and 1.9 m

The axial capacity of built-up CFS box sections was determined from FE analysis. On the other hand, design capacities of CFS built up box section are also calculated as per AISI & AS/NZS for C75 and B75 columns (Table 4). B75-a50-L300-1 specimen with five fasteners failed through local buckling. Some plastic deformations were noticeable near both ends of the stub columns. For most of the short columns of 500 mm length tested, local buckling was noticed. For intermediate and slender columns tested, global buckling was noticeable. Similar behavior was observed for B90 built-up box columns.

The effect of the fastener spacing on compression capacity was investigated and shown in Table 5.The parametric study was further extended by considering three different number of fasteners: 3, 5 and 10 numbers of screws. Length of the built-up box columns was varied from 300 mm to 2000 mm at an increment of 100 mm. In Tables 5(a) and 5(b), the axial capacities determined from the FE analysis were compared against the AISI & AS/NZS design strengths for B75 and B90, respectively. Buckling modes were different when different length and screw spacing were used as shown in Tables 5(a) and 5(b) for B75 and B90, respectively.

5. DESIGN STRENGTHS CALCULATED IN FROM THE AISI & AS/NZS

The FE strengths were compared against the AISI & AS/NZS design capacities for CFS built-up box sections. AISI & AS/NZS uses the Effective Width Method (EWW) while calculating the axial capacity of CFS built-up box columns. According to AISI & AS/NZS, for built-up CFS columns, the axial capacity is calculated as follows:

$$P_{AISI\&AS/NZS} = A_e F_n \quad (1)$$

The critical buckling stress (F_n) was determined as below:

For $\lambda_c \leq 1.5$, $F_n = \left(0.658^{\lambda^2{}_c}\right) F_y$ (2)

For $\lambda_c > 1.5$, $F_n = \left(\frac{0.877}{\lambda^2{}_c}\right) F_y$ (3)

The non-dimensional slenderness (λ_c) is calculated using Eq. (4):

$$\lambda_c = \sqrt{\frac{F_y}{F_e}} \quad (4)$$

Eq. (1) to Eq. (4) can be found in the AISI (2016) standard in section E2, whereas these equations (Eq. (1) to Eq. (4)) can be found in the AS/NZS (2018) standard in section 3.4.1.

Modified slenderness ratio was used for all calculations as per Eq. (5).

$$\left(\frac{KL}{r}\right)_{ms} = \sqrt{\left(\frac{KL}{r}\right)_o^2 + \left(\frac{a}{r_{yc}}\right)^2}\text{; For which } \left(\frac{a}{r_{yc}}\right) \leq 0.5\left(\frac{KL}{r}\right)_o \quad (5)$$

Eq. (5) can be found in the AISI (2016) standard in section I1.2, and in the AS/NZS (2018) standard, this equation (Eq. (5)) can be found in section 4.1.2.

Axial capacities obtained from the FEA and AISI & AS/NZS are compared in Tables 4(a) and 4(b) for B75 and B90 columns, respectively. As can be seen, the AISI & AS/NZS standards are over-conservative while predicting the axial capacities of B75 and B90 columns.

Figure 15(a) shows the FE and design strengths/capacities of the B75 columns against the non-dimensional slenderness. The axial capacities of the columns with 3, 5 and 10 number of screws are shown in Figures 15(a) and 15(b) for B75 and B90 columns, respectively. For reference, experimental strengths were also plotted in Figures 15(a) and 15(b) for B75 and B90, respectively. As can be seen, the FEA results and experimental strengths for all three screw configurations (3, 5 and 10 screws), were higher than the design capacities predicted in accordance with the AISI & AS/NZS. It is also noticeable that the increase number of screws from 5 to 10, affect the design capacities and FEA strengths to be higher (Figure 14(b)). Therefore, it can be concluded that both B75 and B90 series, are conservative by around 17% on average for modified slenderness approach, as prescribed in the AISI & AS/NZS. The average value of P_{FEA} / P_{AISI} & AS/NZS for the B75 stub column is 1.13 with a COV of 0.01 (Table 4(a)).

Figure 15(b) shows the strength of B90 built-up box section with varying non-dimensional slenderness's. As mentioned previously, the design standards are over-conservative by around 17% for B90 columns. From Figures 14(a) and 15(b), when λc was less than 0.3, all columns failed through local buckling while most of the columns failed through global buckling when λc was greater than 0.4. Combined local and global buckling failure were observed for all columns having λc between 0.3 and 0.4.

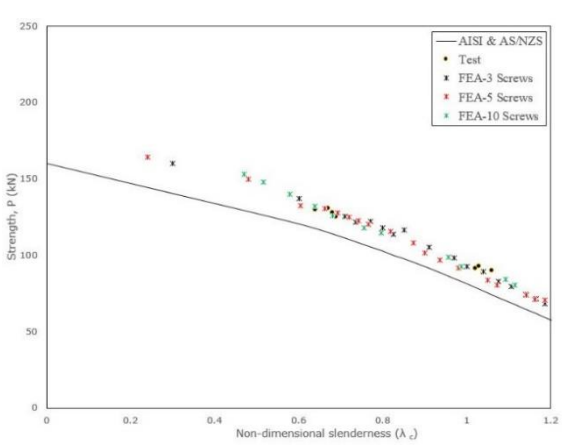

(a) B75

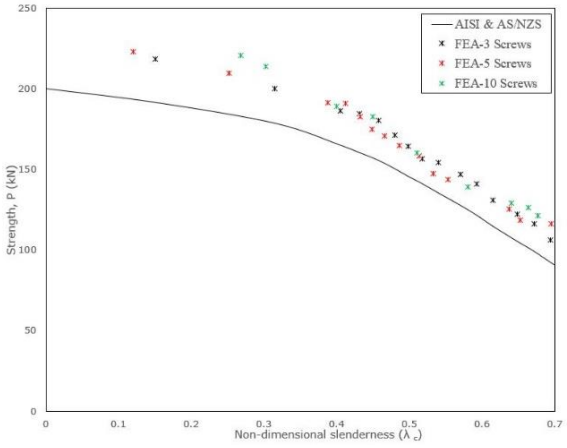

(b) B90

Fig. 15: Comparison between the test, FEA and design strengths calculate in accordance with AISI & AS/NZS with varying number of screws for CFS built-up box sections

6. CONCLUSIONS

This paper presents a numerical investigation on axial capacity of CFS built-up box sections. The finite element package ABAQUS (2018) was used to develop the FE models. The FE models considered material nonlinearities, initial imperfections and modelling of intermediate fasteners. The FE model was validated against the test results recently reported by the authors in another paper. The FE results and test results show good agreement, both in terms of failure loads and deformed shapes.

The validated FE model was then used to conduct a parametric study comprising 148 FE models, to study the effect of fastener spacing on compression capacity of such columns. The axial capacities of the built-up CFS box columns, determined from the experiments and FE analysis are compared against the design strengths/capacities determined from the AISI & AS/NZS design codes. It was found that the AISI & AS/NZS codes are over-conservative to both experimental results and FE results by about 17% for all front-to-front built-up box columns.

References

ABAQUS Analysis User's Manual (2018) - Version **6.14**-2. ABAQUS Inc., USA.

American Iron and Steel Institute (AISI) (2016), "North American Specification for the Design of Cold-formed Steel Structural Members", AISI S100-16.

Australia/New Zealand Standard (AS/NZS) (2018), "Cold-Formed Steel Structures, AS/NZS **4600:2018**, Standards Australia/ Standards New Zealand.

BS EN (2001), Tensile testing of metallic materials method of test at ambient temperature; British Standards Institution

Crisan, A., Ungureanu, V., & Dubina, D. (2014), "Calibration of design formula for buckling strength of built-up back-to-back cold-formed steel members in compression", *7th international conference on thin-walled structures*, Busan, Korea (**Vol. 28**).

Lian, Y., Uzzaman, A., Lim, J. B., Abdelal, G., Nash, D., & Young, B. (2016 a), "Effect of web holes on web crippling strength of cold-formed steel channel sections under end-one-flange loading condition–Part I: Tests and finite element analysis", *Thin-Walled. Struct.*, **107**, 443-452.

Lian, Y., Uzzaman, A., Lim, J. B., Abdelal, G., Nash, D., & Young, B. (2016 b), "Effect of web holes on web crippling strength of cold-formed steel channel sections under end-one-flange loading condition-Part II: Parametric study and proposed design equations", *Thin-Walled. Struct.*, **107**, 489-501.

Rondal, J., & Niazi, M. (1990), "Stability of built-up beams and columns with thin-walled members", *J. Constr. Steel Res*, **16**(4), 329-335.

Roy, K., Ting, T. C. H., Lau, H. H., & Lim, J. B. (2018a), "Effect of thickness on the behaviour of axially loaded back-to-back cold-formed steel built-up channel sections-Experimental and numerical investigation", *Structures*, **16**, 327-346

Roy, K., Ting, T. C. H., Lau, H. H., & Lim, J. B. (2018b), "Nonlinear behaviour of back-to-back gapped built-up cold-formed steel channel sections under compression", *J. Constr. Steel Res*, **147**, 257-276.

Roy, K., Ting, T. C. H., Lau, H. H., & Lim, J. B. (2018c), "Effect of thickness on the behaviour of axially loaded back-to-back cold-formed steel built-up channel sections-Experimental and numerical investigation", *Proceedings of the 'Wei-Wen Yu International Specialty Conference on Cold-Formed Steel Structures*, St. Louis, Missouri, USA.

Roy, K., Ting, T. C. H., Lau, H. H., & Lim, J. B. (2018d), "Nonlinear behavior of axially loaded back-to-back built-up cold-formed steel un-lipped channel sections", *Steel Compos. Struct*, 28 (2), 233-250.

Roy, K., Ting, T. C. H., Lau, H. H., & Lim, J. B. (2019a), "Experimental and numerical investigations on the axial capacity of cold-formed steel built-up box sections", *J. Constr. Steel Res*, **160**, 411-427.

Roy, K., Mohammadjani, C., & Lim, J. B. (2019b), "Experimental and numerical investigation into the behaviour of face-to-face built-up cold-formed steel channel sections under compression", *Thin-Walled. Struct.*, **134**, 291-309.

Roy, K., Lau, H. H., & Lim, J. B. (2019c), "Numerical investigations on the axial capacity of back-to-back gapped built-up cold-formed stainless steel channels", Adv. Struct. Eng, 22, 2289-2310.

Roy, K. & Lim, J. B. (2019d), "Numerical investigation into the buckling behaviour of face-to-face built-up cold-formed stainless steel channel sections under axial compression", *Struct,* **20**, 42-73.

Ting, T. C. H., Roy, K., Lau, H. H., & Lim, J. B. (2018), "Effect of screw spacing on behavior of axially loaded back-to-back cold-formed steel built-up channel sections", *Adv. Struct. Eng*, **21**(3), 474-487.

Young, B., & Ellobody, E. (2005), "Buckling analysis of cold-formed steel lipped angle columns", *J. Struct. Eng.*, **131**(10), 1570-1579.

Young, B., & Ellobody, E. (2007), "Design of cold-formed steel unequal angle compression members", *Thin-Walled. Struct.*, **45**(3), 330-338.

Table 4 Comparison of FEA results against the design strength calculated in accordance with the AISI & AS/NZS for CFS built-up box sections

(a) B75

Specimen	Web d_w (mm)	Flange b_f (mm)	Lip C (mm)	Length L (mm)	Radius R (mm)	Thickness t (mm)	Spacing a (mm)	FEA Results P_{FEA} (kN)	AISI Design Strengths P_{AISI} (kN)	P_{FEA}/P_{AISI} -
Stub										
B75-a50-L300	75.0	40.0	15.0	300.0	1.5	1.0	50.0	164.4	146.8	1.12
B75-a100-L300	75.0	40.0	15.0	300.0	1.5	1.0	100.0	159.9	140.3	1.14
B75-a200-L300	75.0	40.0	15.0	300.0	1.5	1.0	200.0	154.8	137.0	1.13
Mean										1.13
COV										0.01
Short										
B75-a100-L500	75.0	40.0	15.0	500.0	1.5	1.0	100.0	132.6	115.3	1.15
B75-a200-L500	75.0	40.0	15.0	500.0	1.5	1.0	200.0	125.5	111.1	1.13
B75-a400-L500	75.0	40.0	15.0	500.0	1.5	1.0	400.0	119.3	102.9	1.16
Mean										1.15
COV										0.02
Intermediate										
B75-a225-L1000	75.0	40.0	15.0	1000	1.5	1.0	225.0	120.4	102.9	1.17
B75-a450-L1000	75.0	40.0	15.0	1000	1.5	1.0	450.0	116.7	97.6	1.20
B75-a900-L1000	75.0	40.0	15.0	1000	1.5	1.0	900.0	112.5	94.3	1.19
Mean										1.18
COV										0.02
Slender										
B75-a475-L2000	75.0	40.0	15.0	2000	1.5	1.0	475.0	70.4	60.7	1.16
B75-a950-L2000	75.0	40.0	15.0	2000	1.5	1.0	950.0	63.7	56.4	1.13
B75-a1900-L2000	75.0	40.0	15.0	2000	1.5	1.0	1900.0	54.7	47.6	1.15
Mean										1.15
COV										0.02

(b) B90

Specimen	Web d_w (mm)	Flange b_f (mm)	Lip C (mm)	Length L (mm)	Radius R (mm)	Thickness t (mm)	Spacing a (mm)	FEA Results P_{FEA} (kN)	AISI Design Strengths P_{AISI} (kN)	P_{FEA}/P_{AISI} -
Stub										
B90-a50-L300	90.0	50.0	20.0	300.0	1.5	1.0	50.0	198.9	179.2	1.11
B90-a100-L300	90.0	50.0	20.0	300.0	1.5	1.0	100.0	191.9	171.3	1.12
B90-a200-L300	90.0	50.0	20.0	300.0	1.5	1.0	200.0	182.7	158.8	1.15
Mean										1.13
COV										0.02
Short										
B90-a100-L500	90.0	50.0	20.0	500.0	1.5	1.0	100.0	172.9	151.7	1.14
B90-a200-L500	90.0	50.0	20.0	500.0	1.5	1.0	200.0	165.0	142.3	1.16
B90-a400-L500	90.0	50.0	20.0	500.0	1.5	1.0	400.0	159.5	138.7	1.15
Mean										1.15
COV										0.01
Intermediate										
B90-a225-L1000	90.0	50.0	20.0	1000.0	1.5	1.0	225.0	149.3	131.0	1.14
B90-a450-L1000	90.0	50.0	20.0	1000.0	1.5	1.0	450.0	141.2	125.0	1.13
B90-a900-L1000	90.0	50.0	20.0	1000.0	1.5	1.0	900.0	132.8	114.4	1.16
Mean										1.14
COV										0.02
Slender										
B90-a475-L2000	90.0	50.0	20.0	2000.0	1.5	1.0	475.0	92.2	78.8	1.17
B90-a950-L2000	90.0	50.0	20.0	2000.0	1.5	1.0	950.0	81.5	70.9	1.15
B90-a1900-L2000	90.0	50.0	20.0	2000.0	1.5	1.0	1900.0	67.8	58.5	1.16
Mean										1.16
COV										0.01

Table 5 Finite element and AISI & AS/NZS strength with varying length of the CFS built-up box sections for 3, 5 and 10 screws

(a) B75

Specimen	Web	Flange	Lip	Length	Spacing(a)		For	Failure Mode(s)	$P_{AISI\ \&\ AS/NZ}$ for			P_{FEA} for			P_{FEA} / $P_{AISI\ \&\ AS/NZ}$		
	d_w	b_f	C	L	3 screws	5 screws	10 screws		3 screws	5 screws	10 screws	3 screws	5 screws	10 screws	3 screws	5 screws	10 screws
	mm	mm	mm	mm	mm	mm	mm		kN	kN	kN	kN	kN	kN	-	-	-
B75-L300	75.0	40.0	15.0	300	75.0	50.0	27.3	Local	140.3	146.4	168.4	159.9	164.4	186.9	1.14	1.12	1.11
B75-L400	75.0	40.0	15.0	400	100.0	66.7	36.4	Local	120.4	129.7	149.2	137.3	149.7	167.1	1.14	1.15	1.12
B75-L500	75.0	40.0	15.0	500	125.0	83.3	45.5	Local	111.1	115.6	132.9	125.5	132.6	153.2	1.13	1.15	1.15
B75-L600	75.0	40.0	15.0	600	150.0	100.0	54.6	Local	108.7	112.4	129.3	121.7	130.4	147.7	1.12	1.16	1.14
B75-L700	75.0	40.0	15.0	700	175.0	116.7	63.6	Local	105.4	109.2	125.6	122.3	127.8	148.6	1.16	1.17	1.18
B75-L800	75.0	40.0	15.0	800	200.0	133.3	72.7	Local + Flexural	102.6	107.8	124.0	118.0	125.0	145.4	1.15	1.16	1.17
B75-L900	75.0	40.0	15.0	900	225.0	150.0	81.8	Flexural	99.8	104.8	120.5	113.8	122.6	140.1	1.14	1.17	1.16
B75-L1000	75.0	40.0	15.0	1000	250.0	166.7	90.9	Local + Flexural	97.6	102.4	117.8	116.4	120.4	137.8	1.19	1.18	1.17
B75-L1100	75.0	40.0	15.0	1100	275.0	183.3	100.0	Flexural	91.4	97.8	112.5	105.1	115.4	131.9	1.15	1.18	1.17
B75-L1200	75.0	40.0	15.0	1200	300.0	200.0	109.1	Flexural	84.6	92.5	106.4	98.1	108.2	125.9	1.16	1.17	1.18
B75-L1300	75.0	40.0	15.0	1300	325.0	216.7	118.2	Local + Flexural	81.2	88.3	101.5	92.6	101.5	118.1	1.14	1.15	1.16
B75-L1400	75.0	40.0	15.0	1400	350.0	233.3	127.3	Local + Flexural	76.4	83.4	95.9	89.4	96.7	114.5	1.17	1.16	1.19
B75-L1500	75.0	40.0	15.0	1500	375.0	250.0	136.4	Flexural	72.1	77.5	89.1	82.9	91.5	104.5	1.15	1.18	1.17
B75-L1600	75.0	40.0	15.0	1600	400.0	266.7	145.5	Flexural	68.7	72.7	83.6	79.7	83.6	98.9	1.16	1.15	1.18
B75-L1700	75.0	40.0	15.0	1700	425.0	283.3	154.6	Flexural	64.5	68.7	79.0	74.2	80.4	92.7	1.15	1.17	1.17
B75-L1800	75.0	40.0	15.0	1800	450.0	300.0	163.6	Flexural	61.7	64.3	73.9	71.6	73.9	87.5	1.16	1.15	1.18
B75-L1900	75.0	40.0	15.0	1900	475.0	316.7	172.7	Flexural	59.2	62.4	71.8	68.1	71.1	84.2	1.15	1.14	1.17
B75-L2000	75.0	40.0	15.0	2000	500.0	333.3	181.8	Flexural	56.4	60.7	69.8	63.7	70.4	80.4	1.13	1.16	1.15

(a) B90

Specimen	Web	Flange	Lip	Length	Spacing(a)		For	Failure Mode(s)	$P_{AISI\ \&\ AS/NZ}$ for			P_{FEA} for			P_{FEA} / $P_{AISI\ \&\ AS/NZ}$		
	d_w	b_f	C	L	3 screws	5 screws	10 screws		3 screws	5 screws	10 screws	3 screws	5 screws	10 screws	3 screws	5 screws	10 screws
	mm	mm	mm	mm	mm	mm	mm		kN	kN	kN	kN	kN	kN	-	-	-
B90-L300	90.0	50.0	20.0	300	75.0	50.0	27.3	Local	191.5	198.9	222.8	218.3	223.0	249.5	1.14	1.12	1.12
B90-L400	90.0	50.0	20.0	400	100.0	66.7	36.4	Local	178.6	185.6	207.9	200.0	210.0	230.8	1.12	1.13	1.11
B90-L500	90.0	50.0	20.0	500	125.0	83.3	45.5	Local	165.0	172.9	193.6	186.5	200.8	220.8	1.13	1.16	1.14
B90-L600	90.0	50.0	20.0	600	150.0	100.0	54.6	Local	160.4	166.2	186.1	184.5	191.4	214.1	1.15	1.15	1.15
B90-L700	90.0	50.0	20.0	700	175.0	116.7	63.6	Local	155.6	160.1	179.3	180.5	190.8	208.0	1.16	1.19	1.16
B90-L800	90.0	50.0	20.0	800	200.0	133.3	72.7	Local + Flexural	150.4	154.6	173.2	171.5	182.7	197.4	1.14	1.18	1.14
B90-L900	90.0	50.0	20.0	900	225.0	150.0	81.8	Local + Flexural	145.6	149.3	167.2	164.5	174.9	189.0	1.13	1.17	1.13
B90-L1000	90.0	50.0	20.0	1000	250.0	166.7	90.9	Local + Flexural	141.2	144.5	161.8	156.7	170.8	187.7	1.11	1.18	1.16
B90-L1100	90.0	50.0	20.0	1100	275.0	183.3	100.0	Local + Flexural	135.4	139.4	156.1	154.4	164.7	182.7	1.14	1.18	1.17
B90-L1200	90.0	50.0	20.0	1200	300.0	200.0	109.1	Local + Flexural	127.8	133.2	149.2	147.0	158.7	171.6	1.15	1.19	1.15
B90-L1300	90.0	50.0	20.0	1300	325.0	216.7	118.2	Local + Flexural	121.7	125.7	140.8	141.2	147.3	160.5	1.16	1.17	1.14
B90-L1400	90.0	50.0	20.0	1400	350.0	233.3	127.3	Local + Flexural	114.8	119.8	134.2	130.9	144.0	157.0	1.14	1.20	1.17
B90-L1500	90.0	50.0	20.0	1500	375.0	250.0	136.4	Flexural	105.4	111.7	125.1	122.3	132.0	145.1	1.16	1.18	1.16
B90-L1600	90.0	50.0	20.0	1600	400.0	266.7	145.5	Flexural	99.4	105.4	118.0	116.3	125.6	139.3	1.17	1.19	1.18
B90-L1700	90.0	50.0	20.0	1700	425.0	283.3	154.6	Flexural	92.6	100.3	112.3	106.4	118.5	129.2	1.15	1.18	1.15
B90-L1800	90.0	50.0	20.0	1800	450.0	300.0	163.6	Flexural	88.5	97.5	109.2	100.9	116.2	126.7	1.14	1.19	1.16
B90-L1900	90.0	50.0	20.0	1900	475.0	316.7	172.7	Flexural	85.4	95.6	107.1	99.1	113.0	126.3	1.16	1.18	1.18
B90-L2000	90.0	50.0	20.0	2000	500.0	333.3	181.8	Flexural	81.5	92.5	103.6	96.2	107.4	121.2	1.18	1.16	1.17